

Search for the decay $D_s^+ \rightarrow a_0(980)^0 e^+ \nu_e$

M. Ablikim¹, M. N. Achasov^{10,c}, P. Adlarson⁶⁷, S. Ahmed¹⁵, M. Albrecht⁴, R. Aliberti²⁸, A. Amoroso^{66A,66C}, M. R. An³², Q. An^{63,49}, X. H. Bai⁵⁷, Y. Bai⁴⁸, O. Bakina²⁹, R. Baldini Ferroli^{23A}, I. Balossino^{24A}, Y. Ban^{38,k}, K. Begzsuren²⁶, N. Berger²⁸, M. Bertani^{23A}, D. Bettoni^{24A}, F. Bianchi^{66A,66C}, J. Bloms⁶⁰, A. Bortone^{66A,66C}, I. Boyko²⁹, R. A. Briere⁵, H. Cai⁶⁸, X. Cai^{1,49}, A. Calcaterra^{23A}, G. F. Cao^{1,54}, N. Cao^{1,54}, S. A. Cetin^{53A}, J. F. Chang^{1,49}, W. L. Chang^{1,54}, G. Chelkov^{29,b}, D. Y. Chen⁶, G. Chen¹, H. S. Chen^{1,54}, M. L. Chen^{1,49}, S. J. Chen³⁵, X. R. Chen²⁵, Y. B. Chen^{1,49}, Z. J. Chen^{20,l}, W. S. Cheng^{66C}, G. Cibinetto^{24A}, F. Cossio^{66C}, X. F. Cui³⁶, H. L. Dai^{1,49}, X. C. Dai^{1,54}, A. Dbeyssi¹⁵, R. E. de Boer⁴, D. Dedovich²⁹, Z. Y. Deng¹, A. Denig²⁸, I. Denysenko²⁹, M. Destefanis^{66A,66C}, F. De Mori^{66A,66C}, Y. Ding³³, C. Dong³⁶, J. Dong^{1,49}, L. Y. Dong^{1,54}, M. Y. Dong^{1,49,54}, X. Dong⁶⁸, S. X. Du⁷¹, Y. L. Fan⁶⁸, J. Fang^{1,49}, S. S. Fang^{1,54}, Y. Fang¹, R. Farinelli^{24A}, L. Fava^{66B,66C}, F. Feldbauer⁴, G. Felici^{23A}, C. Q. Feng^{63,49}, J. H. Feng⁵⁰, M. Fritsch⁴, C. D. Fu¹, Y. Gao⁶⁴, Y. Gao^{38,k}, Y. Gao^{63,49}, Y. G. Gao⁶, I. Garzia^{24A,24B}, P. T. Ge⁶⁸, C. Geng⁵⁰, E. M. Gersabeck⁵⁸, A. Gilman⁶¹, K. Goetzen¹¹, L. Gong³³, W. X. Gong^{1,49}, W. Gradl²⁸, M. Greco^{66A,66C}, L. M. Gu³⁵, M. H. Gu^{1,49}, S. Gu², Y. T. Gu¹³, C. Y. Guan^{1,54}, A. Q. Guo²², L. B. Guo³⁴, R. P. Guo⁴⁰, Y. P. Guo^{9,h}, A. Guskov²⁹, T. T. Han⁴¹, W. Y. Han³², X. Q. Hao¹⁶, F. A. Harris⁵⁶, N. Hüsken^{22,28}, K. L. He^{1,54}, F. H. Heinsius⁴, C. H. Heinz³⁸, T. Held⁴, Y. K. Heng^{1,49,54}, C. Herold⁵¹, M. Himmelreich^{11,f}, T. Holtmann⁴, Y. R. Hou⁵⁴, Z. L. Hou¹, H. M. Hu^{1,54}, J. F. Hu^{47,m}, T. Hu^{1,49,54}, Y. Hu¹, G. S. Huang^{63,49}, L. Q. Huang⁶⁴, X. T. Huang⁴¹, Y. P. Huang¹, Z. Huang^{38,k}, T. Hussain⁶⁵, W. Ikegami Andersson⁶⁷, W. Imoehl²², M. Irshad^{63,49}, S. Jaeger⁴, S. Janchiv^{26,j}, Q. Ji¹, Q. P. Ji¹⁶, X. B. Ji^{1,54}, X. L. Ji^{1,49}, Y. Y. Ji⁴¹, H. B. Jiang⁴¹, X. S. Jiang^{1,49,54}, J. B. Jiao⁴¹, Z. Jiao¹⁸, S. Jin³⁵, Y. Jin⁵⁷, T. Johansson⁶⁷, N. Kalantar-Nayestanaki⁵⁵, X. S. Kang³³, R. Kappert⁵⁵, M. Kavatsyuk⁵⁵, B. C. Ke^{43,1}, I. K. Keshk⁴, A. Khoukaz⁶⁰, P. Kiese²⁸, R. Kiuchi¹, R. Kliemt¹¹, L. Koch³⁰, O. B. Kolcu^{53A,e}, B. Kopf⁴, M. Kuemmel⁴, M. Kuessner⁴, A. Kupsc⁶⁷, M. G. Kurth^{1,54}, W. Kühn³⁰, J. J. Lane⁵⁸, J. S. Lange³⁰, P. Larin¹⁵, A. Lavania²¹, L. Lavezzi^{66A,66C}, Z. H. Lei^{63,49}, H. Leithoff²⁸, M. Lellmann²⁸, T. Lenz²⁸, C. Li³⁹, C. H. Li³², Cheng Li^{63,49}, D. M. Li⁷¹, F. Li^{1,49}, G. Li¹, H. Li⁴³, H. Li^{63,49}, H. B. Li^{1,54}, H. J. Li¹⁶, J. L. Li⁴¹, J. Q. Li⁴, J. S. Li⁵⁰, Ke Li¹, L. K. Li¹, Lei Li³, P. R. Li³¹, S. Y. Li⁵², W. D. Li^{1,54}, W. G. Li¹, X. H. Li^{63,49}, X. L. Li⁴¹, Xiaoyu Li^{1,54}, Z. Y. Li⁵⁰, H. Liang^{63,49}, H. Liang^{1,54}, H. Liang²⁷, Y. F. Liang⁴⁵, Y. T. Liang²⁵, G. R. Liao¹², L. Z. Liao^{1,54}, J. Libby²¹, C. X. Lin⁵⁰, B. J. Liu¹, C. X. Liu¹, D. Liu^{63,49}, F. H. Liu⁴⁴, Fang Liu¹, Feng Liu⁶, H. B. Liu¹³, H. M. Liu^{1,54}, Huanhuan Liu¹, Huihui Liu¹⁷, J. B. Liu^{63,49}, J. L. Liu⁶⁴, J. Y. Liu^{1,54}, K. Liu¹, K. Y. Liu³³, Ke Liu⁶, L. Liu^{63,49}, M. H. Liu^{9,h}, P. L. Liu¹, Q. Liu⁵⁴, Q. Liu⁶⁸, S. B. Liu^{63,49}, Shuai Liu⁴⁶, T. Liu^{1,54}, W. M. Liu^{63,49}, X. Liu³¹, Y. Liu³¹, Y. B. Liu³⁶, Z. A. Liu^{1,49,54}, Z. Q. Liu⁴¹, X. C. Lou^{1,49,54}, F. X. Lu¹⁶, F. X. Lu⁵⁰, H. J. Lu¹⁸, J. D. Lu^{1,54}, J. G. Lu^{1,49}, X. L. Lu¹, Y. Lu¹, Y. P. Lu^{1,49}, C. L. Luo³⁴, M. X. Luo⁷⁰, P. W. Luo⁵⁰, T. Luo^{9,h}, X. L. Luo^{1,49}, S. Lusso^{66C}, X. R. Lyu⁵⁴, F. C. Ma³³, H. L. Ma¹, L. L. Ma⁴¹, M. M. Ma^{1,54}, Q. M. Ma¹, R. Q. Ma^{1,54}, R. T. Ma⁵⁴, X. X. Ma^{1,54}, X. Y. Ma^{1,49}, F. E. Maas¹⁵, M. Maggiora^{66A,66C}, S. Maldaner⁴, S. Malde⁶¹, Q. A. Malik⁶⁵, A. Mangoni^{23B}, Y. J. Mao^{38,k}, Z. P. Mao¹, S. Marcello^{66A,66C}, Z. X. Meng⁵⁷, J. G. Messchendorp⁵⁵, G. Mezzadri^{24A}, T. J. Min³⁵, R. E. Mitchell²², X. H. Mo^{1,49,54}, Y. J. Mo⁶, N. Yu. Muchnoi^{10,c}, H. Muramatsu⁵⁹, S. Nakhoul^{11,f}, Y. Nefedov²⁹, F. Nerling^{11,f}, I. B. Nikolaev^{10,c}, Z. Ning^{1,49}, S. Nisar^{8,i}, S. L. Olsen⁵⁴, Q. Ouyang^{1,49,54}, S. Pacetti^{23B,23C}, X. Pan^{9,h}, Y. Pan⁵⁸, A. Pathak¹, P. Patteri^{23A}, M. Pelizaeus⁴, H. P. Peng^{63,49}, K. Peters^{11,f}, J. Pettersson⁶⁷, J. L. Ping³⁴, R. G. Ping^{1,49}, R. Poling⁵⁹, V. Prasad^{63,49}, H. Qi^{63,49}, H. R. Qi⁵², K. H. Qi²⁵, M. Qi³⁵, T. Y. Qi⁹, T. Y. Qi², S. Qian^{1,49}, W. B. Qian⁵⁴, Z. Qian⁵⁰, C. F. Qiao⁵⁴, L. Q. Qin¹², X. P. Qin⁹, X. S. Qin⁴¹, Z. H. Qin^{1,49}, J. F. Qiu¹, S. Q. Qu³⁶, K. H. Rashid⁶⁵, K. Ravindran²¹, C. F. Redmer²⁸, A. Rivetti^{66C}, V. Rodin⁵⁵, M. Rolo^{66C}, G. Rong^{1,54}, Ch. Rosner¹⁵, M. Rump⁶⁰, H. S. Sang⁶³, A. Sarantsev^{29,d}, Y. Schelhaas²⁸, C. Schnier⁴, K. Schoenning⁶⁷, M. Scodreggio^{24A,24B}, D. C. Shan⁴⁶, W. Shan¹⁹, X. Y. Shan^{63,49}, J. F. Shanguan⁴⁶, M. Shao^{63,49}, C. P. Shen⁹, P. X. Shen³⁶, X. Y. Shen^{1,54}, H. C. Shi^{63,49}, R. S. Shi^{1,54}, X. Shi^{1,49}, X. D. Shi^{63,49}, J. J. Song⁴¹, W. M. Song^{27,1}, Y. X. Song^{38,k}, S. Sosio^{66A,66C}, S. Spataro^{66A,66C}, K. X. Su⁶⁸, P. P. Su⁴⁶, F. F. Sui⁴¹, G. X. Sun¹, H. K. Sun¹, J. F. Sun¹⁶, L. Sun⁶⁸, S. S. Sun^{1,54}, T. Sun^{1,54}, W. Y. Sun³⁴, W. Y. Sun²⁷, X. Sun^{20,l}, Y. J. Sun^{63,49}, Y. K. Sun^{63,49}, Y. Z. Sun¹, Z. T. Sun¹, Y. H. Tan⁶⁸, Y. X. Tan^{63,49}, C. J. Tang⁴⁵, G. Y. Tang¹, J. Tang⁵⁰, J. X. Teng^{63,49}, V. Thoren⁶⁷, W. H. Tian⁴³, Y. T. Tian²⁵, I. Uman^{53B}, B. Wang¹, C. W. Wang³⁵, D. Y. Wang^{38,k}, H. J. Wang³¹, H. P. Wang^{1,54}, K. Wang^{1,49}, L. L. Wang¹, M. Wang⁴¹, M. Z. Wang^{38,k}, Meng Wang^{1,54}, W. Wang⁵⁰, W. H. Wang⁶⁸, W. P. Wang^{63,49}, X. Wang^{38,k}, X. F. Wang³¹, X. L. Wang¹, Y. Wang⁵⁰, Y. Wang^{63,49}, Y. D. Wang³⁷, Y. F. Wang^{1,49,54}, Y. Q. Wang¹, Y. Y. Wang³¹, Z. Wang^{1,49}, Z. Y. Wang¹, Ziyi Wang⁵⁴, Zongyuan Wang^{1,54}, D. H. Wei¹², P. Weidenkaff²⁸, F. Weidner⁶⁰, S. P. Wen¹, D. J. White⁵⁸, U. Wiedner⁴, G. Wilkinson⁶¹, M. Wolke⁶⁷, L. Wollenberg⁴, J. F. Wu^{1,54}, L. H. Wu¹, L. J. Wu^{1,54}, X. Wu^{9,h}, Z. Wu^{1,49}, L. Xia^{63,49}, H. Xiao^{9,h}, S. Y. Xiao¹, Z. J. Xiao³⁴, X. H. Xie^{38,k}, Y. G. Xie^{1,49}, Y. H. Xie⁶, T. Y. Xing^{1,54}, G. F. Xu¹, Q. J. Xu¹⁴, W. Xu^{1,54}, X. P. Xu⁴⁶, Y. C. Xu⁵⁴, F. Yan^{9,h}, L. Yan^{9,h}, W. B. Yan^{63,49}, W. C. Yan⁷¹, Xu Yan⁴⁶, H. J. Yang^{42,g}, H. X. Yang¹, L. Yang⁴³, S. L. Yang⁵⁴, Y. X. Yang¹², Yifan Yang^{1,54}, Zhi Yang²⁵, M. Ye^{1,49}, M. H. Ye⁷, J. H. Yin¹, Z. Y. You⁵⁰, B. X. Yu^{1,49,54}, C. X. Yu³⁶, G. Yu^{1,54}, J. S. Yu^{20,l}, T. Yu⁶⁴, C. Z. Yuan^{1,54}, L. Yuan², X. Q. Yuan^{38,k}, Y. Yua. Zhang^{1,49}, J. J. Zhang⁴³, J. L. Zhang⁶⁹, J. Q. Zhang³⁴, J. W. Zhang^{1,49,54}, J. Y. Zhang¹, J. Z. Zhang^{1,54}, Jianyu Zhang^{1,54}, Jiawei Zhang^{1,54}, L. M. Zhang¹, K. J. Zhu^{1,49,54}, S. H. Zhu⁶², T. J. Zhu⁶⁹, W. J. Zhu^{9,h}, W. J. Zhu³⁶, Y. C. Zhu^{63,49}, Z. A. Zhu^{1,54}, B. S. Zou¹, J. H. Zou¹

(BESIII Collaboration)

¹ Institute of High Energy Physics, Beijing 100049, People's Republic of China² Beihang University, Beijing 100191, People's Republic of China³ Beijing Institute of Petrochemical Technology, Beijing 102617, People's Republic of China⁴ Bochum Ruhr-University, D-44780 Bochum, Germany⁵ Carnegie Mellon University, Pittsburgh, Pennsylvania 15213, USA

- ⁶ Central China Normal University, Wuhan 430079, People's Republic of China
- ⁷ China Center of Advanced Science and Technology, Beijing 100190, People's Republic of China
- ⁸ COMSATS University Islamabad, Lahore Campus, Defence Road, Off Raiwind Road, 54000 Lahore, Pakistan
- ⁹ Fudan University, Shanghai 200443, People's Republic of China
- ¹⁰ G.I. Budker Institute of Nuclear Physics SB RAS (BINP), Novosibirsk 630090, Russia
- ¹¹ GSI Helmholtzcentre for Heavy Ion Research GmbH, D-64291 Darmstadt, Germany
- ¹² Guangxi Normal University, Guilin 541004, People's Republic of China
- ¹³ Guangxi University, Nanning 530004, People's Republic of China
- ¹⁴ Hangzhou Normal University, Hangzhou 310036, People's Republic of China
- ¹⁵ Helmholtz Institute Mainz, Johann-Joachim-Becher-Weg 45, D-55099 Mainz, Germany
- ¹⁶ Henan Normal University, Xinxiang 453007, People's Republic of China
- ¹⁷ Henan University of Science and Technology, Luoyang 471003, People's Republic of China
- ¹⁸ Huangshan College, Huangshan 245000, People's Republic of China
- ¹⁹ Hunan Normal University, Changsha 410081, People's Republic of China
- ²⁰ Hunan University, Changsha 410082, People's Republic of China
- ²¹ Indian Institute of Technology Madras, Chennai 600036, India
- ²² Indiana University, Bloomington, Indiana 47405, USA
- ²³ INFN Laboratori Nazionali di Frascati, (A)INFN Laboratori Nazionali di Frascati, I-00044, Frascati, Italy; (B)INFN Sezione di Perugia, I-06100, Perugia, Italy; (C)University of Perugia, I-06100, Perugia, Italy
- ²⁴ INFN Sezione di Ferrara, (A)INFN Sezione di Ferrara, I-44122, Ferrara, Italy; (B)University of Ferrara, I-44122, Ferrara, Italy
- ²⁵ Institute of Modern Physics, Lanzhou 730000, People's Republic of China
- ²⁶ Institute of Physics and Technology, Peace Ave. 54B, Ulaanbaatar 13330, Mongolia
- ²⁷ Jilin University, Changchun 130012, People's Republic of China
- ²⁸ Johannes Gutenberg University of Mainz, Johann-Joachim-Becher-Weg 45, D-55099 Mainz, Germany
- ²⁹ Joint Institute for Nuclear Research, 141980 Dubna, Moscow region, Russia
- ³⁰ Justus-Liebig-Universitaet Giessen, II. Physikalisches Institut, Heinrich-Buff-Ring 16, D-35392 Giessen, Germany
- ³¹ Lanzhou University, Lanzhou 730000, People's Republic of China
- ³² Liaoning Normal University, Dalian 116029, People's Republic of China
- ³³ Liaoning University, Shenyang 110036, People's Republic of China
- ³⁴ Nanjing Normal University, Nanjing 210023, People's Republic of China
- ³⁵ Nanjing University, Nanjing 210093, People's Republic of China
- ³⁶ Nankai University, Tianjin 300071, People's Republic of China
- ³⁷ North China Electric Power University, Beijing 102206, People's Republic of China
- ³⁸ Peking University, Beijing 100871, People's Republic of China
- ³⁹ Qufu Normal University, Qufu 273165, People's Republic of China
- ⁴⁰ Shandong Normal University, Jinan 250014, People's Republic of China
- ⁴¹ Shandong University, Jinan 250100, People's Republic of China
- ⁴² Shanghai Jiao Tong University, Shanghai 200240, People's Republic of China
- ⁴³ Shanxi Normal University, Linfen 041004, People's Republic of China
- ⁴⁴ Shanxi University, Taiyuan 030006, People's Republic of China
- ⁴⁵ Sichuan University, Chengdu 610064, People's Republic of China
- ⁴⁶ Soochow University, Suzhou 215006, People's Republic of China
- ⁴⁷ South China Normal University, Guangzhou 510006, People's Republic of China
- ⁴⁸ Southeast University, Nanjing 211100, People's Republic of China
- ⁴⁹ State Key Laboratory of Particle Detection and Electronics, Beijing 100049, Hefei 230026, People's Republic of China
- ⁵⁰ Sun Yat-Sen University, Guangzhou 510275, People's Republic of China
- ⁵¹ Suranaree University of Technology, University Avenue 111, Nakhon Ratchasima 30000, Thailand
- ⁵² Tsinghua University, Beijing 100084, People's Republic of China
- ⁵³ Turkish Accelerator Center Particle Factory Group, (A)Istanbul Bilgi University, 34060 Eyup, Istanbul, Turkey; (B)Near East University, Nicosia, North Cyprus, Mersin 10, Turkey
- ⁵⁴ University of Chinese Academy of Sciences, Beijing 100049, People's Republic of China
- ⁵⁵ University of Groningen, NL-9747 AA Groningen, The Netherlands
- ⁵⁶ University of Hawaii, Honolulu, Hawaii 96822, USA
- ⁵⁷ University of Jinan, Jinan 250022, People's Republic of China
- ⁵⁸ University of Manchester, Oxford Road, Manchester, M13 9PL, United Kingdom
- ⁵⁹ University of Minnesota, Minneapolis, Minnesota 55455, USA
- ⁶⁰ University of Muenster, Wilhelm-Klemm-Str. 9, 48149 Muenster, Germany
- ⁶¹ University of Oxford, Keble Rd, Oxford, UK OX13RH
- ⁶² University of Science and Technology Liaoning, Anshan 114051, People's Republic of China
- ⁶³ University of Science and Technology of China, Hefei 230026, People's Republic of China
- ⁶⁴ University of South China, Hengyang 421001, People's Republic of China
- ⁶⁵ University of the Punjab, Lahore-54590, Pakistan
- ⁶⁶ University of Turin and INFN, (A)University of Turin, I-10125, Turin, Italy; (B)University of Eastern Piedmont, I-15121,

Alessandria, Italy; (C)INFN, I-10125, Turin, Italy

⁶⁷ Uppsala University, Box 516, SE-75120 Uppsala, Sweden

⁶⁸ Wuhan University, Wuhan 430072, People's Republic of China

⁶⁹ Xinyang Normal University, Xinyang 464000, People's Republic of China

⁷⁰ Zhejiang University, Hangzhou 310027, People's Republic of China

⁷¹ Zhengzhou University, Zhengzhou 450001, People's Republic of China

^a Also at Bogazici University, 34342 Istanbul, Turkey

^b Also at the Moscow Institute of Physics and Technology, Moscow 141700, Russia

^c Also at the Novosibirsk State University, Novosibirsk, 630090, Russia

^d Also at the NRC "Kurchatov Institute", PNPI, 188300, Gatchina, Russia

^e Also at Istanbul Arel University, 34295 Istanbul, Turkey

^f Also at Goethe University Frankfurt, 60323 Frankfurt am Main, Germany

^g Also at Key Laboratory for Particle Physics, Astrophysics and Cosmology, Ministry of Education; Shanghai Key Laboratory for Particle Physics and Cosmology; Institute of Nuclear and Particle Physics, Shanghai 200240, People's Republic of China

^h Also at Key Laboratory of Nuclear Physics and Ion-beam Application (MOE) and Institute of Modern Physics, Fudan University, Shanghai 200443, People's Republic of China

ⁱ Also at Harvard University, Department of Physics, Cambridge, MA, 02138, USA

^j Currently at: Institute of Physics and Technology, Peace Ave.54B, Ulaanbaatar 13330, Mongolia

^k Also at State Key Laboratory of Nuclear Physics and Technology, Peking University, Beijing 100871, People's Republic of China

^l School of Physics and Electronics, Hunan University, Changsha 410082, China

^m Also at Guangdong Provincial Key Laboratory of Nuclear Science, Institute of Quantum Matter, South China Normal University, Guangzhou 510006, China

Using 6.32 fb^{-1} of electron-positron collision data recorded by the BESIII detector at center-of-mass energies between 4.178 and 4.226 GeV, we present the first search for the decay $D_s^+ \rightarrow a_0(980)^0 e^+ \nu_e$, $a_0(980)^0 \rightarrow \pi^0 \eta$, which could proceed via $a_0(980)$ - $f_0(980)$ mixing. No significant signal is observed. An upper limit of 1.2×10^{-4} at the 90% confidence level is set on the product of the branching fractions of $D_s^+ \rightarrow a_0(980)^0 e^+ \nu_e$ and $a_0(980)^0 \rightarrow \pi^0 \eta$ decays.

I. INTRODUCTION

The constituent quark model has been strikingly successful in the past few decades. The nonets of pseudo-scalar, vector and tensor mesons are now well identified. On the other hand, the classification of $J^{\text{PC}} = 0^{++}$ scalar mesons still faces difficulty, because there are more states than predicted by the quark model. Many theoretical hypotheses have been proposed to explain these extra states, such as the tetraquark states, two-meson bound states, molecular-like states, etc. [1]. More experimental results are crucial to sort out the interpretations of these states. Semileptonic meson decays have a relatively simple decay mechanism and final state interactions and can provide a clean probe for studying their hadronic part. In particular, semileptonic D meson decays with one scalar meson in the final state provide an ideal opportunity to investigate the internal structures of these light states [2, 3]. Example studies of this type are the semileptonic decays: $D^+ \rightarrow f_0(500)e^+\nu_e$, $D^+ \rightarrow f_0(980)e^+\nu_e$, $D^{0(+)} \rightarrow a_0(980)^{-(0)}e^+\nu_e$, and $D_s^+ \rightarrow f_0(980)e^+\nu_e$ [4–8]. However, the decay $D_s^+ \rightarrow a_0(980)^0 e^+ \nu_e$ has not yet been studied.

The D_s^+ direct decay to $a_0(980)^0 e^+ \nu_e$ violates isospin invariance, but it may occur from $D_s^+ \rightarrow f_0(980)e^+\nu_e$ via $a_0(980)$ - $f_0(980)$ mixing. BESIII has observed $a_0(980)$ - $f_0(980)$ mixing and measured its intensity to be 0.4% in

the decays of $J/\psi \rightarrow \phi f_0(980) \rightarrow \phi a_0(980)^0$ and $\chi_{cJ} \rightarrow f_0(980)\pi^0 \rightarrow a_0(980)^0\pi^0$ [9]. With the product branching fractions (BF) $\mathcal{B}(D_s^+ \rightarrow f_0(980)e^+\nu_e) \times \mathcal{B}(f_0(980) \rightarrow \pi^+\pi^-) = (0.13 \pm 0.02 \pm 0.01) \times 10^{-2}$ [6] and assuming $a_0(980)$ - $f_0(980)$ mixing effects are the same for J/ψ , χ_{cJ} and D_s^+ decays, one may estimate a BF on the order of 10^{-5} for $D_s^+ \rightarrow a_0(980)^0 e^+ \nu_e$.

A study of the decay $D_s^+ \rightarrow a_0(980)^0 e^+ \nu_e$ could provide important information on $a_0(980)$ - $f_0(980)$ mixing and help to understand the nature of the scalar meson $a_0(980)$ in the charm sector. In this paper, the process of $D_s^+ \rightarrow a_0(980)^0 e^+ \nu_e$ with $a_0(980)^0 \rightarrow \pi^0 \eta$ is studied based on 6.32 fb^{-1} of data recorded by the BESIII detector at center-of-mass energies (\sqrt{s}) between 4.178 and 4.226 GeV. A blind analysis is performed to avoid a possible bias. Throughout this paper, charge conjugate channels are always implied.

II. DETECTOR AND DATA SETS

Details about the BESIII detector are described elsewhere [10, 11]. In short, it is a magnetic spectrometer located at the Beijing Electron Positron Collider (BEPCII) [12]. The cylindrical core of the BESIII detector consists of a helium-based multilayer drift chamber (MDC), a plastic scintillator time-of-flight sys-

tem (TOF), and a CsI(Tl) electromagnetic calorimeter (EMC), which are all enclosed in a superconducting solenoidal magnet providing a 1.0 T magnetic field. The solenoid is supported by an octagonal flux-return yoke with resistive plate counter muon identifier modules interleaved with steel. The acceptance of charged particles and photons is 93% over 4π solid angle. The charged-particle momenta resolution at 1.0 GeV/c is 0.5%, and the specific energy loss (dE/dx) resolution is 6% for electrons from Bhabha scattering. The EMC measures photon energies with a resolution of 2.5% (5%) at 1 GeV in the barrel (end cap) region. The time resolution of the TOF barrel part is 68 ps, while that of the end cap part is 110 ps. The end cap TOF was upgraded in 2015 with multi-gap resistive plate chamber technology, providing a time resolution of 60 ps [13].

Data samples used in this analysis correspond to an integrated luminosity (\mathcal{L}_{int}) of 6.32 fb^{-1} taken in the range of $\sqrt{s} = 4.178 - 4.226 \text{ GeV}$, as listed in Table I, and provide a large sample of D_s^\pm mesons from $D_s^{*\pm} D_s^\mp$ events. The cross section of $D_s^{*\pm} D_s^\mp$ production in e^+e^- annihilation is about a factor of twenty larger than that of $D_s^+ D_s^-$ [14] and $D_s^{*\pm}$ decays to γD_s^\pm with a dominant BF of $(93.5 \pm 0.7)\%$ [1].

TABLE I. The integrated luminosity \mathcal{L}_{int} and the recoil mass M_{rec} requirements for various energies, where M_{rec} is defined in Eq. 5. The first and second uncertainties are statistical and systematic, respectively.

\sqrt{s} (GeV)	\mathcal{L}_{int} (pb $^{-1}$)	M_{rec} (GeV/ c^2)
4.178	$3189.0 \pm 0.2 \pm 31.9$	[2.050, 2.180]
4.189	$526.7 \pm 0.1 \pm 2.2$	[2.048, 2.190]
4.199	$526.0 \pm 0.1 \pm 2.1$	[2.046, 2.200]
4.209	$517.1 \pm 0.1 \pm 1.8$	[2.044, 2.210]
4.219	$514.6 \pm 0.1 \pm 1.8$	[2.042, 2.220]
4.226	$1047.3 \pm 0.1 \pm 10.2$	[2.040, 2.220]

Simulated Monte-Carlo (MC) samples produced with GEANT4-based [15] software, which includes the geometric description of the BESIII detector and the detector response, are used to determine the detection efficiency and to estimate the background contributions. The simulation includes the beam energy spread and initial state radiation (ISR) in the e^+e^- annihilation modeled with the generator KKMC [16]. Generic MC samples are used to simulate the background contributions and consist of the production of $D\bar{D}$ pairs including quantum coherence for all neutral D modes, non- $D\bar{D}$ decays of the $\psi(3770)$, ISR production of the J/ψ and $\psi(3686)$ states, and continuum processes. The known decay modes are modeled with EVENTGEN [17] using world averaged BF values [1], and the remaining unknown decays from the charmonium states with LUNDCHARM [18]. Final state radiation from charged final state particles is incorporated with PHOTOS [19]. The signal detection efficiencies and signal shapes are obtained from signal MC sam-

ples, in which the signal decay $D_s^+ \rightarrow a_0(980)^0 e^+ \nu_e$, $a_0(980)^0 \rightarrow \pi^0 \eta$, is simulated using an MC generator where the amplitude of the $a_0(980)^0$ meson follows a theoretical $a_0(980)$ - $f_0(980)$ mixing model [3, 20–22]. This amplitude is given by $A_{\text{mix}} = \frac{D_{fa}}{D_f D_a}$, in which D_a and D_f are the $a_0(980)$ and $f_0(980)$ propagators, respectively, and $D_{fa} = \frac{g_{a_0 K^+ K^-} g_{f_0 K^+ K^-}}{16\pi} \times i[\rho_{K^+ K^-}(s) - \rho_{K^0 \bar{K}^0}(s)]$. Here, $\rho_{K\bar{K}}(s)$ is the velocity of the K meson in the rest frame of its mother particle, and $g_{a_0 K^+ K^-}$ and $g_{f_0 K^+ K^-}$ are coupling constants [22].

III. DATA ANALYSIS

The signal process $e^+e^- \rightarrow D_s^{*+} D_s^- + c.c. \rightarrow \gamma D_s^+ D_s^- + c.c$ allows studying semileptonic D_s^\pm decays with a tag technique [23] since only one neutrino escapes undetected. There are two types of samples used in the tag technique: single tag (ST) and double tag (DT). In the ST sample, a D_s^- meson is reconstructed through a particular hadronic decay without any requirement on the remaining measured tracks and EMC showers. In the DT sample, a D_s^- , designated as “tag”, is reconstructed through a decay mode first, and then a D_s^+ , designated as the “signal”, is reconstructed with the remaining tracks and EMC showers. For one tag mode, the ST yield is given by

$$N_{\text{tag}}^{\text{ST}} = 2N_{D_s^* D_s} \mathcal{B}_{\text{tag}} \epsilon_{\text{tag}}^{\text{ST}}, \quad (1)$$

and the DT yield is given by

$$N_{\text{tag,sig}}^{\text{DT}} = 2N_{D_s^* D_s} \mathcal{B}_\gamma \mathcal{B}_{\text{tag}} \mathcal{B}_{\text{sig}} \epsilon_{\text{tag,sig}}^{\text{DT}}, \quad (2)$$

where $N_{D_s^* D_s}$ is the total number of $D_s^{*+} D_s^- + c.c.$ pairs produced, $\mathcal{B}_{\text{sig}(\text{tag})}$ is the BF of the signal decay (the tag mode), \mathcal{B}_γ is the BF of $D_s^* \rightarrow \gamma D_s$, and ϵ denotes the corresponding reconstruction efficiencies. By isolating \mathcal{B}_{sig} , one obtains:

$$\mathcal{B}_{\text{sig}} = \frac{N_{\text{tag,sig}}^{\text{DT}} \epsilon_{\text{tag}}^{\text{ST}}}{\mathcal{B}_\gamma N_{\text{tag}}^{\text{ST}} \epsilon_{\text{tag,sig}}^{\text{DT}}}, \quad (3)$$

where the yields $N_{\text{tag}}^{\text{ST}}$ and $N_{\text{tag,sig}}^{\text{DT}}$ can be obtained from data samples, while $\epsilon_{\text{tag}}^{\text{ST}}$ and $\epsilon_{\text{tag,sig}}^{\text{DT}}$ can be obtained from generic and signal MC samples, respectively. The above equations can be generalized for multiple tag modes and multiple values of \sqrt{s} :

$$\mathcal{B}_{\text{sig}} = \frac{N_{\text{total,sig}}^{\text{DT}}}{\mathcal{B}_\gamma \sum_{\alpha,i} N_{\alpha,i}^{\text{ST}} \epsilon_{\alpha,i}^{\text{DT}} / \epsilon_{\alpha,i}^{\text{ST}}}, \quad (4)$$

where α represents tag modes, i represents different \sqrt{s} , and $N_{\text{total,sig}}^{\text{DT}}$ is the total signal yield.

The tag candidates are reconstructed with charged K and π , π^0 , $\eta^{(\prime)}$, and K_S^0 mesons which satisfy the particle selection detailed below. Twelve tag modes are used and the requirements on the mass of tagged D_s^- (M_{tag}) are summarized in Table II.

Photons are reconstructed from clusters found in the EMC. The EMC shower time is required to be within $[0, 700]$ ns from the event start time in order to suppress fake photons due to electronic noise or e^+e^- beam background. Photon candidates within $|\cos\theta| < 0.80$ (barrel) are required to deposit more than 25 MeV of energy, and those with $0.86 < |\cos\theta| < 0.92$ (end cap) must deposit more than 50 MeV, where θ is the polar angle with respect to the z axis, which is the symmetry axis of the MDC. To suppress Bremsstrahlung photons from charged tracks, the directions of photon candidates must be at least 10° away from all charged tracks. The π^0 (η) candidates are reconstructed through $\pi^0 \rightarrow \gamma\gamma$ ($\eta \rightarrow \gamma\gamma$) decays, with at least one barrel photon. The diphoton invariant masses for the identification of π^0 and η decays are required to be in the range $[0.115, 0.150]$ GeV/ c^2 and $[0.490, 0.580]$ GeV/ c^2 , respectively. The χ^2 of a 1C kinematic fit constraining $M_{\gamma\gamma}$ to the π^0 or η nominal mass [1] should be less than 30.

Charged track candidates reconstructed using the information of the MDC must satisfy $|\cos\theta| < 0.93$ with the closest approach to the interaction point less than 10 cm in the z direction and less than 1 cm in the plane perpendicular to z . Charged tracks are identified as pions or kaons with particle identification (PID), which is implemented by combining the information of dE/dx of the MDC and the time-of-flight from the TOF system. For charged kaon (pion) candidates, the probability for the kaon (pion) hypothesis is required to be larger than that for a pion (kaon). For electron identification, the dE/dx , TOF information and EMC measurements are used to construct likelihoods for electron, pion, and kaon hypotheses (\mathcal{L}_e , \mathcal{L}_π , and \mathcal{L}_K). Electron candidates must satisfy $\mathcal{L}_e/(\mathcal{L}_e + \mathcal{L}_\pi + \mathcal{L}_K) > 0.7$. Additionally, the energy measurement using the EMC information of the electron candidate has to be more than 80% of the track momentum measured by the MDC ($E/cp > 0.8$).

Candidate K_S^0 mesons are reconstructed with pairs of two oppositely charged tracks, whose distances of closest approach along z are less than 20 cm. The invariant masses of these charged track pairs are required to be within $[0.487, 0.511]$ GeV/ c^2 . The ρ^0 candidates are selected via the process $\rho^0 \rightarrow \pi^+\pi^-$ with an invariant mass window $[0.570, 0.970]$ GeV/ c^2 . The η' candidates are formed from $\pi^+\pi^-\eta$ and $\gamma\rho^0$ combinations with invariant masses falling within the range of $[0.946, 0.970]$ and $[0.936, 0.976]$ GeV/ c^2 , respectively.

In order to identify the process $e^+e^- \rightarrow D_s^{*\pm}D_s^\mp$, the signal windows, listed in Table I, are applied to the recoiling mass (M_{rec}) of the tag candidate. The definition

of M_{rec} is

$$\frac{1}{c^2} \sqrt{(E_{cm} - \sqrt{c^2|\vec{p}_{\text{tag}}|^2 + c^4m_{D_s}^2})^2 - c^2|\vec{p}_{cm} - \vec{p}_{\text{tag}}|^2} \quad (5)$$

where $(E_{cm}/c, \vec{p}_{cm}) \equiv p_{cm}$ is the four-momentum of the e^+e^- center-of-mass system, $(\frac{1}{c}\sqrt{|\vec{p}_{\text{tag}}|^2 + m_{D_s}^2}, \vec{p}_{\text{tag}}) \equiv p_{\text{tag}}$ is the measured four momentum of the tag candidate, and m_{D_s} is the nominal D_s^- mass [1]. If there are multiple candidates for a tag mode, the one with M_{rec} closest to $D_s^{*\pm}$ mass [1] is chosen.

The ST yields for tag modes $N_{\text{tag}}^{\text{ST}}$ are obtained by fitting the distributions of the tag D_s^- invariant mass (M_{tag}). Example fits to data samples at 4.178 GeV are shown in Fig. 1. The fitting function is an incoherent sum of the signal and the background contributions. The description of the signal is based on the MC-simulated shape convolved with a Gaussian function. The background is described by a second-order Chebyshev polynomial function. Based on MC studies, in all the tag modes, the only significant peaking background is from $D^- \rightarrow K_S^0\pi^-$ and $D_s^- \rightarrow \eta\pi^+\pi^-\pi^-$ decays faking the $D_s^- \rightarrow K_S^0K^-$ and $D_s^- \rightarrow \pi^-\eta'$ tag modes, respectively. For these cases, MC simulated shapes of the two peaking backgrounds are added to the background polynomial functions. The ST yields of data sample and ST efficiencies for tag modes are listed in Table II.

After a tag D_s^- is identified, we search for the signal $D_s^+ \rightarrow a_0(980)^0 e^+ \nu_e$, $a_0(980)^0 \rightarrow \pi^0\eta$ recoiling against the tag by requiring one charged track identified as e^+ and at least five more photons (two for π^0 , two for η , and one to reconstruct the transition photon of $D_s^{*\pm} \rightarrow \gamma D_s^\pm$). Events having tracks other than those accounted for in the tagged D_s^- and the electron are rejected ($N_{\text{char}}^{\text{extra}} = 0$). Kinematic fits are performed on $e^+e^- \rightarrow D_s^{*\pm}D_s^\mp \rightarrow \gamma D_s^+ D_s^-$ with D_s^- decays to one of the tag modes and D_s^+ decays to the signal mode. The combination with the minimum χ^2 assuming a D_s^{*+} meson decays to $D_s^+\gamma$ or a D_s^{*-} meson decays to $D_s^-\gamma$ is chosen. The total four-momentum is constrained to the four-momentum of e^+e^- . Invariant masses of the D_s^- tag, the D_s^+ signal, and the D_s^* are constrained to the corresponding nominal masses [1]. Furthermore, it is required that the maximum energy of photons not used in the DT event selection ($E_{\gamma, \text{max}}^{\text{extra}}$) is less than 0.2 GeV. Whether the photon forms a D_s^{*-} candidate with the tag D_s^- or a D_s^{*+} candidate with the signal D_s^+ , the square of the recoil mass against the photon and the D_s^- tag ($M_{\text{rec}}'^2$) should peak at the nominal D_s^\pm meson mass-squared before the kinematics fit for signal $D_s^{*\pm}D_s^\mp$ events. Therefore, we require $M_{\text{rec}}'^2$ to satisfy $3.80 < M_{\text{rec}}'^2 < 4.00$ GeV $^2/c^4$, as shown in Fig. 2(a). To select events from the $a_0(980)^0$ signal region, the invariant mass of $\pi^0\eta$ ($M_{\pi^0\eta}$) is required to satisfy $0.95 < M_{\pi^0\eta} < 1.05$ GeV/ c^2 , as shown in Fig. 2(b).

The missing neutrino is reconstructed by the missing mass squared (MM^2), defined as

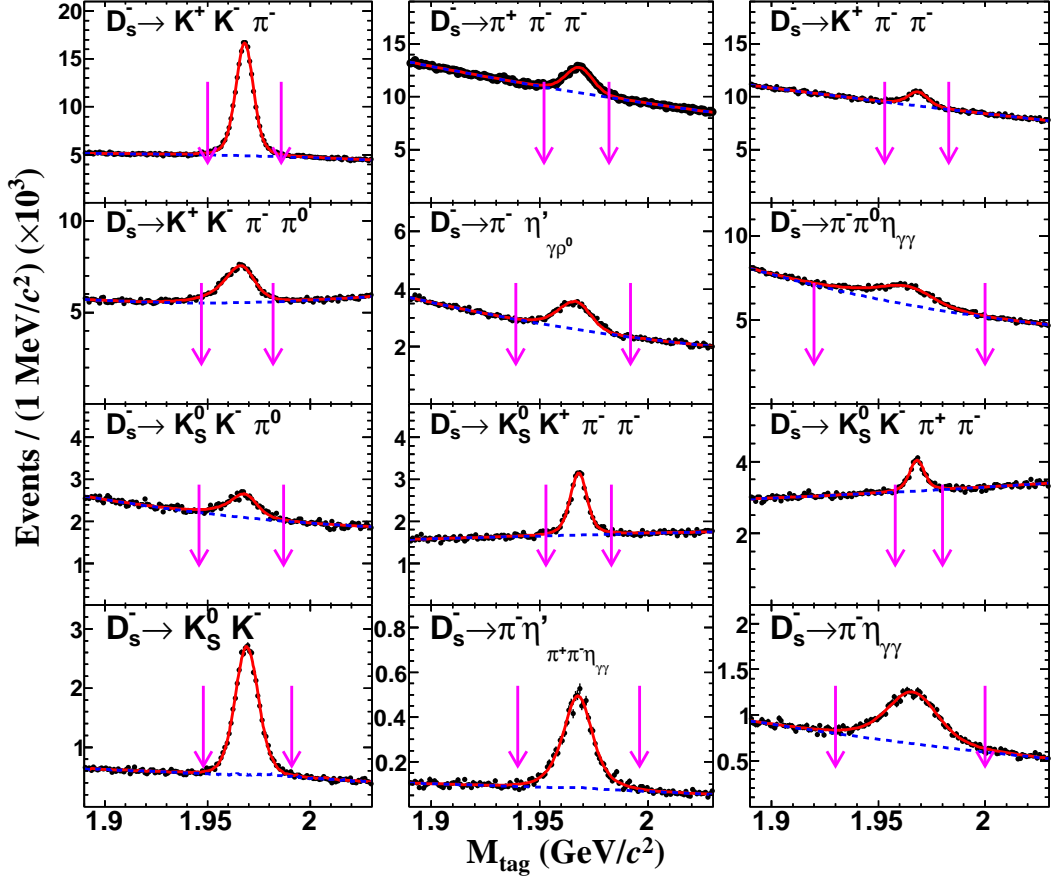


FIG. 1. Fits to D_s^- mass distributions of ST data samples at $\sqrt{s} = 4.178$ GeV. The points with error bars are data, red solid lines are total fits, and blue dashed lines are background. The pairs of pink arrows denote signal regions. MC simulated shapes of $D^- \rightarrow K_S^0 \pi^-$ and $D_s^- \rightarrow \eta \pi^+ \pi^- \pi^-$ decays are added to the background polynomial functions in the fits of $D_s^- \rightarrow K_S^0 K^-$ and $D_s^- \rightarrow \pi^- \eta'$ decays to account for the peaking background, respectively.

TABLE II. Requirements on M_{tag} , the ST yields ($N_{\text{tag}}^{\text{ST}}$) and ST efficiencies ($\epsilon_{\text{tag}}^{\text{ST}}$) for energy points, (I) $\sqrt{s} = 4.178$ GeV, (II) 4.189-4.219 GeV, and (III) 4.226 GeV, where the subscripts of η and η' denote the decay modes used to reconstruct η and η' . The efficiencies for the energy points 4.189-4.219 GeV are averaged based on the luminosities. The BF's of the sub-particle (K_S^0 , π^0 , η and η') decays are not included. Uncertainties are statistical only.

Tag mode	M_{tag} (GeV/ c^2)	(I) $N_{\text{tag}}^{\text{ST}}$	(I) $\epsilon_{\text{tag}}^{\text{ST}}$ (%)	(II) $N_{\text{tag}}^{\text{ST}}$	(II) $\epsilon_{\text{tag}}^{\text{ST}}$ (%)	(III) $N_{\text{tag}}^{\text{ST}}$	(III) $\epsilon_{\text{tag}}^{\text{ST}}$ (%)
$D_s^- \rightarrow K^+ K^- \pi^-$	[1.950, 1.986]	135859 ± 612	38.96 ± 0.03	80418 ± 503	38.81 ± 0.04	28287 ± 327	38.24 ± 0.07
$D_s^- \rightarrow K_S^0 K^-$	[1.948, 1.991]	31716 ± 273	48.89 ± 0.06	18310 ± 227	46.86 ± 0.08	6542 ± 143	46.36 ± 0.15
$D_s^- \rightarrow \pi^- \eta_{\gamma\gamma}$	[1.930, 2.000]	18119 ± 609	43.07 ± 0.15	10224 ± 458	42.48 ± 0.21	3708 ± 253	41.75 ± 0.40
$D_s^- \rightarrow \pi^- \eta'_{\pi^+ \pi^- \eta_{\gamma\gamma}}$	[1.940, 1.996]	7799 ± 139	19.01 ± 0.06	4468 ± 111	18.96 ± 0.07	1675 ± 64	18.88 ± 0.13
$D_s^- \rightarrow K^+ K^- \pi^- \pi^0$	[1.947, 1.982]	38550 ± 772	10.15 ± 0.03	22945 ± 641	10.22 ± 0.04	7900 ± 437	10.23 ± 0.08
$D_s^- \rightarrow \pi^- \pi^- \pi^+$	[1.952, 1.982]	37702 ± 852	50.71 ± 0.15	21517 ± 777	49.61 ± 0.21	7622 ± 542	49.39 ± 0.42
$D_s^- \rightarrow K_S^0 K^+ \pi^- \pi^-$	[1.953, 1.983]	15637 ± 287	21.74 ± 0.06	8903 ± 233	21.57 ± 0.08	3240 ± 172	21.28 ± 0.15
$D_s^- \rightarrow \rho_{\pi^- \pi^0}^- \eta$	[1.920, 2.000]	41113 ± 1324	17.81 ± 0.10	25742 ± 1203	17.89 ± 0.14	10729 ± 1450	17.45 ± 0.28
$D_s^- \rightarrow \pi^- \eta'_{\gamma\rho^0}$	[1.939, 1.992]	20173 ± 603	25.36 ± 0.11	11364 ± 514	25.47 ± 0.15	3763 ± 727	25.52 ± 0.29
$D_s^- \rightarrow K^- \pi^+ \pi^-$	[1.953, 1.983]	16939 ± 544	45.80 ± 0.22	10121 ± 456	45.38 ± 0.30	4918 ± 432	44.75 ± 0.57
$D_s^- \rightarrow K_S^0 K^- \pi^0$	[1.946, 1.987]	11260 ± 516	15.09 ± 0.11	6792 ± 469	14.76 ± 0.15	2128 ± 226	14.84 ± 0.27
$D_s^- \rightarrow K_S^0 K^- \pi^+ \pi^-$	[1.958, 1.980]	8013 ± 270	20.29 ± 0.12	5257 ± 289	20.97 ± 0.15	1708 ± 219	19.45 ± 0.30

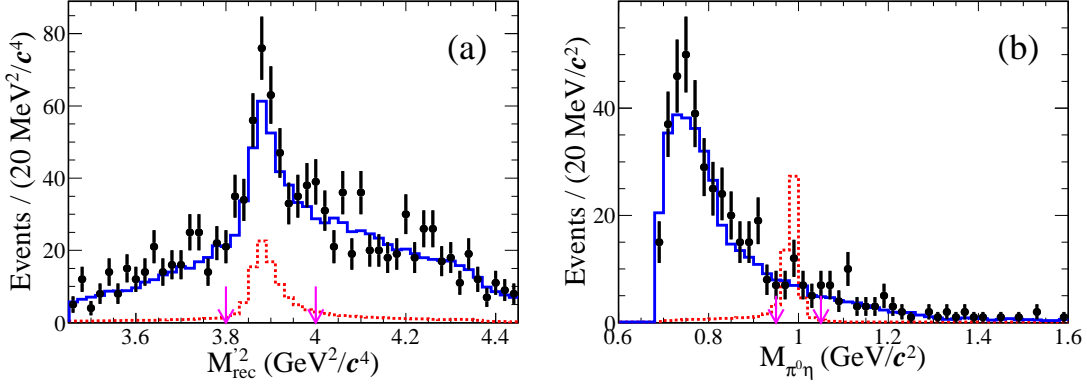


FIG. 2. (a) $M_{\text{rec}}'^2$ and (b) $M_{\pi^0\eta}$ distributions of data and MC samples at $\sqrt{s} = 4.178\text{--}4.226$ GeV. The pair of pink arrows denotes the signal windows. The points with error bars are data. The blue solid and the red dashed lines are generic and signal MC samples, respectively. The signal MC is normalized arbitrarily for visualization purposes. A missing mass cut, $|MM^2| < 0.35$ GeV $^2/c^4$, is applied.

$$MM^2 = \frac{1}{c^2}(p_{cm} - p_{\text{tag}} - p_{\pi^0} - p_{\eta} - p_e - p_{\gamma})^2, \quad (6)$$

where p_i ($i = \pi^0, \eta, e, \gamma$) is the four-momentum of the daughter particle i on the signal side. The MM^2 distribution of accepted candidate events is shown in Fig. 3. The DT efficiencies are obtained using the signal MC samples and listed in Table III. Since no significant sig-

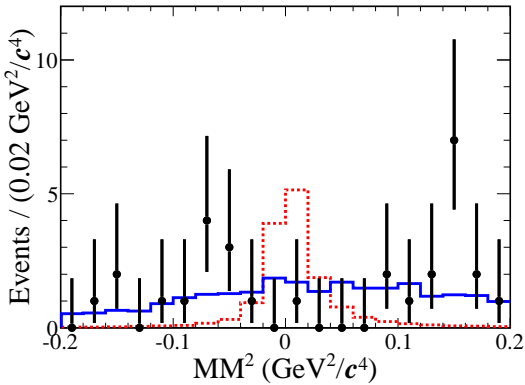


FIG. 3. MM^2 distributions of data and MC samples at $\sqrt{s} = 4.178\text{--}4.226$ GeV in the signal window. The points with error bars are data. The blue solid and the red dashed lines are generic and signal MC samples, respectively. The signal MC is normalized arbitrarily for visualization purposes.

nal is observed, an upper limit is determined. Maximum-likelihood fits to the MM^2 distribution are performed, and likelihoods are determined as a function of assumed BF. The signal and the background shapes are modeled by MC-simulated shapes obtained from the signal MC and the generic MC samples, respectively. The likelihood distribution versus BF is shown in Fig. 4.

IV. SYSTEMATIC UNCERTAINTY

Systematic uncertainties on the BF measurement are summarized in Table IV and the sources are classified into two types: multiplicative (σ_e) and additive. Note that most systematic uncertainties on the tag side cancel due to the tag technique.

Multiplicative uncertainties are from the efficiency determination and the quoted BFs. The uncertainty from the BFs of $D_s^* \rightarrow \gamma D_s$ and $\pi^0/\eta \rightarrow \gamma\gamma$ decays are set to be 0.8% and 0.5%, respectively, according to the world averaged values [1]. The systematic uncertainties from tracking and PID efficiency of the e^\pm , assigned as 1.0%, are studied by analyzing radiative Bhabha events. The systematic uncertainties from reconstruction efficiencies of neutral particles are determined to be 2% for π^0 and η by studying a control sample of $\psi(3770) \rightarrow D\bar{D}$ with hadronic D decays, and 1% for γ by studying a control sample of $J/\psi \rightarrow \pi^+\pi^-\pi^0$ [24, 25]. The uncertainties of the $E_{\gamma, \text{max}}^{\text{extra}} < 0.2$ GeV and $N_{\text{char}}^{\text{extra}} = 0$ requirements are assigned as 0.5% and 0.9%, respectively, by analyzing DT hadronic events, whereby one D_s^\mp decays into one of the tag modes and the other D_s^\pm decays into $K^+K^-\pi^\pm$ or $K_S K^\pm$. The parameters of the $a_0(980)\text{--}f_0(980)$ mixing model in generating the signal MC samples are varied by $\pm 1\sigma$, and the change of signal efficiency is assigned as the systematic uncertainty. By adding these uncertainties in quadrature, the total uncertainty σ_e is estimated to be 4.7%.

Additive uncertainties affect the signal yield determination, which is dominated by the imperfect background shape description. The systematic uncertainty is studied by altering the nominal MC background shape with two methods. First, alternative MC shapes are used, where the relative fractions of backgrounds from the major background source $D_s^+ \rightarrow \eta e\nu$, $q\bar{q}$, and non- $D_s^{*+}D_s^-$ open-charm are varied within their uncertainties. Sec-

TABLE III. The DT efficiencies ($\epsilon_{\text{tag,sig}}^{\text{DT}}$) for energy points, (I) $\sqrt{s} = 4.178$ GeV, (II) 4.189-4.219 GeV, and (III) 4.226 GeV. The efficiencies for the energy points 4.189-4.219 GeV are averaged based on the luminosities. The BF's of the sub-particle (K_S^0 , π^0 , η and η') decays are not included. Uncertainties are statistical only.

Tag mode	(I) $\epsilon_{\text{tag,sig}}^{\text{DT}}(\%)$	(II) $\epsilon_{\text{tag,sig}}^{\text{DT}}(\%)$	(III) $\epsilon_{\text{tag,sig}}^{\text{DT}}(\%)$
$D_s^- \rightarrow K^+ K^- \pi^-$	4.51 ± 0.03	4.36 ± 0.02	4.17 ± 0.03
$D_s^- \rightarrow K_S^0 K^-$	5.67 ± 0.08	5.42 ± 0.04	5.00 ± 0.08
$D_s^- \rightarrow \pi^- \eta$	5.63 ± 0.09	5.46 ± 0.05	4.85 ± 0.09
$D_s^- \rightarrow \pi^- \eta'_{\pi^+\pi^-\eta}$	2.41 ± 0.06	2.32 ± 0.03	2.16 ± 0.06
$D_s^- \rightarrow K^+ K^- \pi^- \pi^0$	1.26 ± 0.02	1.25 ± 0.01	1.19 ± 0.02
$D_s^- \rightarrow \pi^+ \pi^- \pi^-$	6.25 ± 0.07	5.92 ± 0.04	5.64 ± 0.07
$D_s^- \rightarrow K_S^0 K^+ \pi^- \pi^-$	2.55 ± 0.05	2.42 ± 0.02	2.31 ± 0.04
$D_s^- \rightarrow \rho_{\pi^-\pi^0}^- \eta$	1.76 ± 0.02	1.68 ± 0.01	1.52 ± 0.02
$D_s^- \rightarrow \pi^- \pi'_{\gamma\rho^0}$	3.66 ± 0.06	3.49 ± 0.03	3.26 ± 0.06
$D_s^- \rightarrow K^- \pi^+ \pi^-$	5.48 ± 0.09	5.12 ± 0.04	4.79 ± 0.09
$D_s^- \rightarrow K_S^0 K^- \pi^0$	2.01 ± 0.04	1.95 ± 0.02	1.84 ± 0.04
$D_s^- \rightarrow K_S^0 K^- \pi^+ \pi^-$	2.36 ± 0.06	2.26 ± 0.03	2.22 ± 0.06

TABLE IV. The multiplicative systematic uncertainties.

Source	σ_ϵ (%)
$\mathcal{B}(D_s^* \rightarrow \gamma D_s)$	0.8
$\mathcal{B}(\pi^0/\eta \rightarrow \gamma\gamma)$	0.5
e^+ Tracking efficiency	1.0
e^+ PID efficiency	1.0
π^0/η reconstruction	4.0
γ reconstruction	1.0
$E_{\gamma,\text{max}}^{\text{extra}} < 0.2$ GeV	0.5
MC statistics	0.5
$N_{\text{char}}^{\text{extra}} = 0$	0.9
Signal model	1.0
Total	4.7

ond, the background shape is obtained from the generic MC sample using a kernel estimation method [26] implemented in RooFit [27]. The smoothing parameter of RooKeysPdf is varied to be 0, 1, and 2 to obtain alternative background shapes.

V. RESULTS

Since the additive uncertainty is obtained with very limited sample size, it very likely does not obey a Gaussian distribution and must be considered conservatively. We repeat the maximum-likelihood fits by varying the background shape and take the most conservative upper limit among different choices of background shapes. To incorporate the multiplicative systematic uncertainty in the calculation of the upper limit, the likelihood distribution is smeared by a Gaussian function with a mean of

zero and a width equal to σ_ϵ as below [28, 29]

$$L(n) \propto \int_0^1 L(n \frac{\epsilon}{\epsilon_0}) \exp[-\frac{(\epsilon - \epsilon_0)^2}{2\sigma_\epsilon^2}] d\epsilon, \quad (7)$$

where $L(n)$ is the likelihood distribution as a function of the yield n and ϵ_0 is the averaged efficiency.

The red solid and blue dashed curves in Fig. 4 show the updated and the raw likelihood distributions, respectively. The upper limit on the BF at the 90% confidence level, obtained by integrating from zero to 90% of the resulting curve, is $\mathcal{B}(D_s^+ \rightarrow a_0(980)^0 e^+ \nu_e) \times \mathcal{B}(a_0(980)^0 \rightarrow \pi^0 \eta) < 1.2 \times 10^{-4}$.

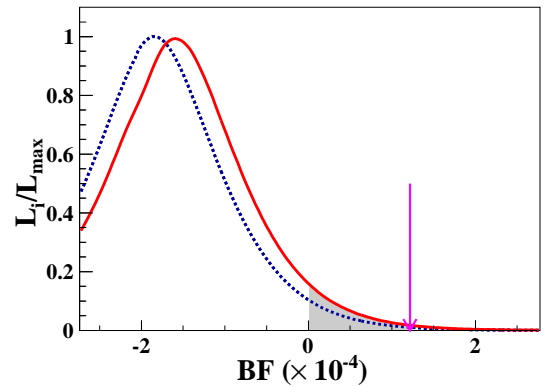


FIG. 4. Overlays of likelihood distributions versus BF of data samples at $\sqrt{s} = 4.178$ -4.226 GeV. The results obtained with and without incorporating the systematic uncertainties are shown in red solid and blue dashed curves, respectively. The pink arrow shows the result corresponding to the 90% confidence level.

VI. CONCLUSION

Using 6.32 fb^{-1} of data taken at $\sqrt{s} = 4.178\text{--}4.226 \text{ GeV}$ and recorded by the BESIII detector at BEPCII, we perform the first search for $D_s^+ \rightarrow a_0(980)^0 e^+ \nu_e$ and obtain an upper limit on $\mathcal{B}(D_s^+ \rightarrow a_0(980)^0 e^+ \nu_e) \times \mathcal{B}(a_0(980)^0 \rightarrow \pi^0 \eta) < 1.2 \times 10^{-4}$ at the 90% confidence level. No obvious isospin violation is observed. Comparing to the estimated BF on the order of 10^{-5} , this first study of $a_0(980)$ - $f_0(980)$ mixing in the charm sector shows no conflict with the BESIII $a_0(980)$ - $f_0(980)$ mixing measurement results in J/ψ and χ_{cJ} decays [9].

ACKNOWLEDGMENTS

The BESIII collaboration thanks the staff of BEPCII and the IHEP computing center for their strong support. This work is supported in part by National Key Research and Development Program of China under Contracts Nos. 2020YFA0406300, 2020YFA0406400; National Natural Science Foundation of China (NSFC) under Contracts Nos. 11625523, 11635010, 11735014, 11822506, 11835012, 11875054, 11935015, 11935016, 11935018,

11961141012; the Chinese Academy of Sciences (CAS) Large-Scale Scientific Facility Program; Joint Large-Scale Scientific Facility Funds of the NSFC and CAS under Contracts Nos. U1732263, U1832207, U2032104; CAS Key Research Program of Frontier Sciences under Contracts Nos. QYZDJ-SSW-SLH003, QYZDJ-SSW-SLH040; 100 Talents Program of CAS; INPAC and Shanghai Key Laboratory for Particle Physics and Cosmology; ERC under Contract No. 758462; European Union Horizon 2020 research and innovation programme under Contract No. Marie Skłodowska-Curie grant agreement No 894790; German Research Foundation DFG under Contracts Nos. 443159800, Collaborative Research Center CRC 1044, FOR 2359, FOR 2359, GRK 214; Istituto Nazionale di Fisica Nucleare, Italy; Ministry of Development of Turkey under Contract No. DPT2006K-120470; National Science and Technology fund; Olle Engkvist Foundation under Contract No. 200-0605; STFC (United Kingdom); The Knut and Alice Wallenberg Foundation (Sweden) under Contract No. 2016.0157; The Royal Society, UK under Contracts Nos. DH140054, DH160214; The Swedish Research Council; U. S. Department of Energy under Contracts Nos. DE-FG02-05ER41374, DE-SC-0012069.

-
- [1] P. A. Zyla *et al.* (Particle Data Group), Prog. Theor. Exp. Phys. **2020**, 083C01 (2020).
 - [2] W. Wang, Phys. Lett. B **759**, 501 (2016).
 - [3] W. Wang and C. D. Lu, Phys. Rev. D **82**, 034016 (2010).
 - [4] J. Yelton *et al.* (CLEO Collaboration), Phys. Rev. D **80**, 052007 (2009).
 - [5] K. M. Ecklund *et al.* (CLEO Collaboration), Phys. Rev. D **80**, 052009 (2009).
 - [6] J. Hietala *et al.*, Phys. Rev. D **92**, 012009 (2015).
 - [7] M. Ablikim *et al.* (BESIII Collaboration), Phys. Rev. Lett. **121**, 081802 (2018).
 - [8] M. Ablikim *et al.* (BESIII Collaboration), Phys. Rev. Lett. **122**, 062001 (2019).
 - [9] M. Ablikim *et al.* (BESIII Collaboration), Phys. Rev. Lett. **121**, 022001 (2018).
 - [10] M. Ablikim *et al.* (BESIII Collaboration), Nucl. Instrum. Methods Phys. Res. Sect. A **614**, 345 (2010).
 - [11] M. Ablikim *et al.* (BESIII Collaboration), Chin. Phys. C **44**, 040001 (2020).
 - [12] C. H. Yu *et al.*, Proceedings of IPAC2016, Busan, Korea, 2016, doi:10.18429/JACoW-IPAC2016-TUYA01.
 - [13] X. Li *et al.*, Radiat. Detect. Technol. Methods **1**, 13 (2017); Y. X. Guo *et al.*, Radiat. Detect. Technol. Methods **1**, 15 (2017); P. Cao *et al.*, Nucl. Instrum. Meth. A **953**, 163053 (2020).
 - [14] D. Cronin-Hennessy *et al.* (CLEO Collaboration), Phys. Rev. D **80**, 072001 (2009).
 - [15] S. Agostinelli *et al.* (GEANT4 Collaboration), Nucl. Instrum. Meth. A **506**, 250 (2003).
 - [16] S. Jadach *et al.*, Phys. Rev. D **63**, 113009 (2001).
 - [17] D. J. Lange, Nucl. Instrum. Meth. A **462**, 152 (2001); R. G. Ping, Chin. Phys. C **32**, 599 (2008).
 - [18] J. C. Chen *et al.*, Phys. Rev. D **62**, 034003 (2000); R. L. Yang *et al.*, Chin. Phys. Lett. **31**, 061301 (2014).
 - [19] E. Richter-Was, Phys. Rev. D **62**, 034003 (2000).
 - [20] N. N. Achasov *et al.*, Phys. Lett. **88B**, 367 (1979).
 - [21] J. J. Wu, Q. Zhao, and B. S. Zou, Phys. Rev. D **75**, 114012 (2007).
 - [22] J. J. Wu and B. S. Zou, Phys. Rev. D **78**, 074017 (2008).
 - [23] J. Adler *et al.* (MARK-III Collaboration), Phys. Rev. Lett. **62**, 1821 (1989).
 - [24] M. Ablikim *et al.* (BESIII Collaboration), Eur. Phys. J. C **76**, 369 (2016).
 - [25] M. Ablikim *et al.* (BESIII Collaboration), Chin. Phys. C **40**, 113001 (2016).
 - [26] K. S. Cranmer, Comput. Phys. Commun. **136**, 198 (2001).
 - [27] R. Brun and F. Rademakers, Nucl. Instrum. Methods Phys. Res., Sect. A **389**, 81 (1997).
 - [28] K. Stenson, arXiv:0605236[physics].
 - [29] X. X. Liu, X. R. Lyu, and Y. S. Zhu, Chin. Phys. C **39**, 113001 (2015).